Received: 17 October 2022 | Revised: 4 January 2023 | Accepted: 14 January 2023

DOI: 10.1002/aic.18053

AIChE JOURNAL

RESEARCH ARTICLE

Editor's Choice: Thermodynamics and Molecular-Scale Phenomena

Aromatic volatile organic compounds absorption with phenyl-based deep eutectic solvents: A molecular thermodynamics and dynamics study

Gangqiang Yu[1,2] | Nicolás F. Gajardo-Parra[2] | Min Chen[1] | Biaohua Chen[1] | Gabriele Sadowski[2] | Christoph Held[2]

[1]Faculty of Environment and Life, Beijing University of Technology, Beijing, China

[2]Laboratory of Thermodynamics, Department of Biochemical and Chemical Engineering, TU Dortmund University, Dortmund, Germany

Correspondence
Biaohua Chen, Faculty of Environment and Life, Beijing University of Technology, 100 Ping Le Yuan, Chaoyang District, Beijing 100124, China.
Email: chenbh@bjut.edu.cn

Gabriele Sadowski and Christoph Held, Laboratory of Thermodynamics, Department of Biochemical and Chemical Engineering, TU Dortmund University, Emil-Figge-Street 70, 44227 Dortmund, Germany.
Email: gabriele.sadowski@tu-dortmund.de and christoph.held@tu-dortmund.de

Funding information
Deutsche Forschungsgemeinschaft, Grant/Award Number: 390677874; Deutscher Akademischer Austauschdienst, Grant/Award Number: 57516591; National Natural Science Foundation of China, Grant/Award Number: 22008003; China Scholarship Council, Grant/Award Number: 202206545009

Abstract

The suitability of phenyl-based deep eutectic solvents (DESs) as absorbents for toluene absorption was investigated by means of thermodynamic modeling and molecular dynamics (MD). The thermodynamic models perturbed-chain statistical associating fluid theory (PC-SAFT) and conductor-like screening model for real solvents (COSMO-RS) were used to predict the vapor–liquid equilibrium of DES–toluene systems. PC-SAFT yielded quantitative results even without using any binary fitting parameters. Among the five DESs studied in this work, [TEBAC][PhOH] consisting of triethyl benzyl ammonium chloride (TEBAC) and phenol (PhOH), was considered as the most suitable absorbent. Systems with [TEBAC][PhOH] had lowest equilibrium pressures of the considered DES–toluene mixtures, the best thermodynamic characteristics (i.e., Henry's law constant, excess enthalpy, Gibbs free energy of solvation of toluene), and the highest self-diffusion coefficient of toluene. The molecular-level mechanism was explored by MD simulations, indicating that [TEBAC][PhOH] has the strongest interaction of DES–toluene compared to the other DESs under study. This work provides guidance to rationally design novel DESs for efficient aromatic volatile organic compounds absorption.

KEYWORDS
COSMO-RS model, deep eutectic solvent, molecular dynamics simulation, PC-SAFT model, VOC absorption

1 | INTRODUCTION

There are many kinds of volatile organic compounds (VOCs) in the atmosphere with complex sources such as combustion of fossil energy, transportation, locomotive emission, chemical process, organic solvents.[1,2] Typical VOCs are classified into aromatic hydrocarbons, alkanes, olefins, lipids, aldehydes, and so forth.[3–6] Aromatic hydrocarbons, as an important category of atmospheric VOCs, mainly come from anthropogenic sources, such as vehicle emissions and factory solvent evaporation, leakage of petrochemical, and packaging and printing. Aromatic VOCs play an important role in atmospheric photochemical oxidation and contribute to the formation of ozone and secondary organic aerosol in the atmosphere.[7–9] In the stratosphere, ozone can effectively protect human beings and the environment.

However, in the troposphere, the increase in ozone concentration will cause a series of impacts on human health and the ecological environment.[7] Moreover, aromatic VOCs have strong toxicity and can directly cause harm to the human nervous system, cardiovascular system, immune system, kidney, liver, and so forth; some substances even have strong carcinogenic effects.[3] Thus, it is urgent to treatment or eliminate aromatic VOCs for the purpose of both environmental protection and human health. At present, the treatment methods of VOCs can be divided into two categories: destructive methods (e.g., catalytic combustion, plasma, and biological oxidation),[10–15] and recovery methods (e.g., adsorption, absorption, and membrane separation).[16–22] The most widely used of the former is catalytic combustion, which is essentially a redox reaction with the help of a catalyst to convert organic matter into CO_2 and water. The technology is limited the application for low-concentration and single-component VOC streams, the lifetime and selectivity of the catalyst is a challenge, and the additional CO_2 emissions are generated. The recycling method is a sustainable VOCs treatment method currently advocated. In addition to the effective treatment of VOCs to solve environmental problems, it can also be recycled and reused economically through absorbent regeneration, which is conducive to the development of carbon neutrality and circular economy.[23,24] In the VOCs recovery technologies, the absorption method is widely used in industry due to its simple operation, mature technologies, and wide application range. The absorbent is usually a high-boiling organic solvent (such as diisobutyl phthalate, hexadecane, and silicone oil).[25] However, the absorption process has problems such as loss of absorbent volatility, and high energy consumption for absorbent regeneration. This shows that the existing VOCs absorption technology currently is realized at the expense of high material consumption and high energy consumption, so it is necessary to develop high-performance "green absorbents" to replace of traditional organic solvents for breaking through the bottleneck of current absorption technologies.

Over a few decades, ionic liquids (ILs) as a type of tunable solvent have received an extensive attention to focusing on chemical separation fields,[26–28] such as CO_2 capture,[29–31] NH_3,[32] H_2S and SO_2 absorption,[31] and solvent extraction due to their unique physicochemical properties like negligible volatility and high solubility and selectivity to specific gases compared to conventional absorbents. There are some researches on using ILs to absorb VOCs,[33,34] for example, the IL [EMIM][Tf_2N] which can effectively absorb benzene, toluene, and *p*-xylene.[35] Using [EMIM][Tf_2N] to absorb sulfur-containing VOCs (dimethyl sulfide and dimethyl disulfide) based on the absorption tower, the experimental capture efficiency is as high as 90%.[36] In addition, some functionalized ILs containing π-electron donors were developed to further enhance the absorption performance of toluene.[37] In short, the advantage of VOC absorption technology with ILs compared with traditional absorbent technology is that the former has no solvent loss. At the same time, it can simplify the absorption process and reduce the energy consumption of absorbent regeneration through using flash regeneration with the low-energy demand in IL processes to replace of high-energy distillation regeneration in conventional absorbent processes. However, in the synthesis process, the more complex synthesis steps of ILs, and the purification process with higher energy and material consumption lead to higher production costs when compared with conventional solvents, at the same time, the former have worse environmental impact compared to the latter. Therefore, this limits the large-scale application of ILs in VOCs absorption.[38,39]

Deep eutectic solvents (DESs) are a new type of eutectic mixed solvents formed by the complexation of hydrogen bond acceptors (HBAs) and hydrogen bond donors (HBDs).[40] DESs are similar with ILs in many properties such as negligible volatility, wide liquid range, high electrical conductivity, low surface tension and high solubility to organics and inorganics and so forth. When compared with ILs, DESs as have the unique advantages like simple preparation, low toxicity, biodegradability, and biocompatibility, thus, it can be treated as the so-called "green solvents." Due to these advantages, they have become a new type of alternatives to ILs in chemical processes,[41,42] such as gas absorption,[43] drug dissolution,[44] metal extraction,[45] and spent lithium-ion battery recycling.[46] There are a few related studies on VOCs absorption with DESs reported. For instance, Chen et al.[47] studied the absorption of acetone by using hydrophobic thymol-based DESs, and results indicated that the DES thymol:decanoic acid (1:1) ([Thy][DecA]) demonstrated very high acetone absorption capacity up to 6.57 mg/g DES at 20°C and 1480 ppm acetone, and the absorption capacity hardly changes with increasing the alkyl chain length the HBD due to the decisive effect of HB interaction between acetone and thymol. Mu et al.[48] employed the phosphonium-based DESs to absorb dichloromethane, indicating that the absorption capacity of dichloromethane in the DES tetrabutylphosphonium chloride: levulinic acid (1:2) ([P_{4444}][Cl][LA]) can be up to 899 mg/g DES at 30°C. Song et al.[49] found that the toluene absorption capacity in the oleic acid-based DESs is comparable with imidazolium-based ILs. Anyway, there are relatively few reports on capturing VOCs absorption, especially aromatic VOCs by using DESs. Almost all the reported studies only focus on the experimental absorption performance of VOCs, its thermodynamic behaviors such as phase equilibrium, thermodynamic analyses (e.g., absorption enthalpy and free energy), the HBA/HBD structural effect on the VOC absorption capacity and the molecular-level microscopic absorption mechanism are not understood enough up still now.

It was found that introducing the π-electron donors into the DESs can intensify the toluene absorption capacity in previous publication.[50] Although some molecular-level insights into intensification mechanisms dominated by the π-electron related interaction between IL–toluene and DES–toluene based on the single molecular cluster at gas phase conditions were given by using quantum chemical (QC) calculations, the microscopic intermolecular interactions, structural distributions and molecular diffusions at the bulk molecule level based on the molecular dynamics (MD) simulation are missing. This will serve as a promising theoretical guide for screening and designing DESs from the enormous HBA/HBD family to implement the efficient VOCs absorption. Moreover, thermodynamic phase behaviors of DES–toluene systems can provide the basic data for process design and optimization of toluene absorption through establishing the

equilibrium stage model, but also reveal structure–property relationship between the microscopic properties (e.g., molecular groups, weak interactions, structural distributions of HBAs/HBDs) and macroscopic features (e.g., absorption capacity and Henry's law constants). It is very time-consuming by trial-and-error experimental measurements, thus, it is needed to resort to thermodynamic models, which are a bridge between microstructures and macroscopic properties. In this work, the perturbed-chain statistical associating fluid theory (PC-SAFT) equations of state,[51,52] and the conductor-like screening model for real solvents (COSMO-RS) model[53] were employed to predict the thermodynamic properties of the DES–VOC systems.

In this work, toluene was chosen as a representative aromatic VOC studied, five ammonium-based DESs ([TEBAC][PhOH], [TEAC][PhOH], [TEBAC][LA], [TAAC][PhOH], and [TEBAC][EG]) with phenyl groups consisted of three HBAs (i.e., TEBAC, TEAC and TAAC) and three HBDs (i.e., PhOH, LA and EG), corresponding full names and abbreviations are illustrated in Supporting Information. The work focuses on addressing the following research issues: (i) identifying the structure–property relationship between DES (i.e., HBA and HBD) structures and vapor–liquid equilibrium (VLE) of DES–toluene systems; (ii) determining whether the PC-SAFT and COSMO-RS models can be extended to predict the VLE of DES–toluene systems; (iii) exploring the effect of DES (i.e., HBA and HBD) structures on the thermodynamic characteristics (i.e., Henry's constants, excess enthalpy of toluene, and the Gibbs free energy of solvation of toluene in DESs); (iv) carrying out MD simulations of five DES–toluene systems to unravel the molecular interactions of HBA–/HBD–/DES–toluene, structural distributions of and diffusion behaviors of HBAs, HBDs, and toluene at the bulk micro-molecular level. This work will help systematically understand the VLE behavior of DES–toluene systems from the viewpoints of the relationship between DES (HBA/HBD) structures and thermodynamic behaviors, weak interactions, molecular distributions, and dynamic diffusions at the molecular level, aiming to provide theoretical guidance for rational design of novel DESs for the highly efficient VOC absorption, and facilitates DES applications in the field of gas separation.

2 | EXPERIMENTAL SECTIONS

2.1 | Materials

TEBAC, TEAC, and TAAC treated as three HBAs, and EG, LA, and PhOH treated as three HBAs were used in this work. The details (e.g., full names, abbreviations, purity of chemicals, and suppliers) for all the chemicals involved in this work are summarized in Table S1, and they were directly used as received without any processing.

2.2 | Synthesis of DESs

In this work, five DESs of [TEBAC][PhOH], [TEAC][PhOH], [TEBAC][LA], [TAAC][PhOH], and [TEBAC][EG] at the fixed molar ratio of HBA:HBD = 1:2 were synthesized by simply physical mixing HBAs and HBDs. The synthesized DESs were purified and dehydrated in a vacuum dryer (Shanghai Yiheng Scientific Instrument Co., Ltd.) at 333.15 K with the water content less than 0.04 wt% through the Karl–Fischer titration. The DES structures were validated by the ^{1}HMR spectra (Figure S1). Densities and viscosities of five DESs were determined via Anton Paar DMA 4500 M automatic analyzer (see Figure S2 for corresponding results). Their thermophysical properties were determined via TGA 209 Libra (NETZSCH Germany) at a heating rate of 10 K/min under N_2 atmosphere (see Figure S3 for corresponding results).

2.3 | VLE experiment

The VLE data of DES–toluene systems were experimentally obtained over a wide range of temperature by using the approach of measuring vapor pressures. The details for measuring VLE of DES–toluene systems are shown in Supporting Information Section "Vapor–liquid equilibrium (VLE) experiment", and the corresponding experimental device is shown in Figure S4. It should be noted that each experimental point was determined three times to ensure the reliability of data. The accuracy of experimental approach and device was validated by measuring saturated vapor pressure of pure toluene as shown in Figure S5.

3 | THERMODYNAMIC MODELING AND THEORETICAL CALCULATIONS

For the toluene (1) + DES (2) systems, the VLE equation is written as

$$y_1 P \phi_1^{V}(T,P,y_1) = x_1 \gamma_1^{L} P_1^{LV} \quad (1)$$

where x_1 and y_1 are the molar fractions of toluene in liquid and vapor phases, respectively; and $y_1 = 1$ because of ultralow volatility of DESs. $\phi_1^{V}(T,P,y_1)$ is the fugacity coefficient of toluene in the vapor phase at the given system temperature T and pressure P, and $\phi_1^{V}(T,P,y_1) = 1$ because of the low pressure. The vapor pressure of pure liquid toluene, P_1^{LV} at the given T was calculated by the Antoine equation.[54] γ_1^{L} is the activity coefficient of toluene in DESs obtained by using the PC-SAFT and COSMO-RS models.

3.1 | PC-SAFT model

PC-SAFT equation of state was used to describe the experimental VLE data of DES–toluene systems, as it is widely used in the literature to represent phase equilibrium.[55–57] A full description of PC-SAFT is available in the original references.[51,52] SAFT models express the dimensionless residual Helmholtz energy (a^{res}) as a sum of contributions representing different inter-molecular interactions based on the existing thermodynamic perturbation

Component	m_i^{seg}	σ_i	u_i/k_B	N_i^{assoc}	ε^{AiBi}/k_B	k^{AiBi}
[TEBAC][PhOH] (1:2)	2.889	4.131	502.02	1:1	5000	0.1
[TEAC][PhOH] (1:2)	2.647	3.706	327.287	1:1	5000	0.1
[TEBAC][LA] (1:2)	3.290	4.041	450.225	1:1	5000	0.1
[TAAC][PhOH] (1:2)	2.939	3.743	370.136	1:1	5000	0.1
[TEBAC][EG] (1:2)	2.371	4.186	599.923	1:1	5000	0.1
Toluene[51]	2.815	3.717	285.69	0	0	0

TABLE 1 PC–SAFT parameters of toluene and the DESs used in this work.

theories.[58,59] In this work, original PC-SAFT was used, as expressed in Equation (2):

$$a^{res} = a - a^{id} = a^{hc} + a^{disp} + a^{assoc} \tag{2}$$

where the superscripts in Equation (2) concern the ideal (id), hard chain (hc), dispersion (disp), and association (assoc) contributions to the residual Helmholtz energy, respectively. These contributions, in turn, are functions of the following adjustable parameters: the segment number, m_i^{seg}, the segment diameter, σ_i, the dispersion-energy parameter, u_i/k_B, where k_B is the Boltzmann constant, the association-energy parameter, ε^{AiBi}/k_B, the association-volume parameter, k^{AiBi}, and the number of association sites, N_i^{assoc}. In this work, DESs were modeled as associative compounds with a 2B association scheme according to the nomenclature of Huang and Radosz.[60] In order to reduce the number of adjustable parameters of the PC-SAFT for DESs, the association volume, and association energy parameters were set to $k^{AiBi} = 0.1$ and $\varepsilon^{AiBi}/k_B = 5000$ K, respectively, as suggested in the literature.[56,57] The three remaining pure–component parameters were estimated by experimental liquid-density data of the DESs measured in this work (see Figure S6 for density correlation); meanwhile, toluene parameters were retrieved from the literature.[51] All pure-component PC-SAFT parameters used in this work are reported in Table 1. The parameters for mixtures are determined by the conventional Berthelot–Lorentz combining rules, as shown in Equations (3) and (4). In this work, we used the value of $k_{ij} = 0$ to predict the VLE of DES–toluene systems. In addition, the mixture parameters of the association-energy (ε^{AiBi}) and the association-volume (k^{AiBi}) parameters were determined as proposed by Wolbach and Sandler,[61] shown in Equations (5) and (6).

$$\sigma_{ij} = \frac{1}{2}(\sigma_i + \sigma_j) \tag{3}$$

$$u_{ij} = \sqrt{u_i u_j}(1 - k_{ij}) \quad k_{ij} = 0 \text{ in this work} \tag{4}$$

$$\varepsilon^{A_iB_j} = \frac{1}{2}\left(\varepsilon^{A_iB_i} + \varepsilon^{A_jB_j}\right) \tag{5}$$

$$k^{A_iB_j} = \sqrt{k^{A_iB_i}k^{A_jB_j}}\left(\frac{\sqrt{\sigma_i\sigma_j}}{1/2(\sigma_i + \sigma_j)}\right) \tag{6}$$

The activity coefficient of component i in the liquid mixture γ_i^L was obtained by the following relation

$$\gamma_i^L = \varphi_i^L / \varphi_{0i}^L \tag{7}$$

where φ_i^L and $\varphi_{0i}^L \varphi_{0i}^L$ represent the fugacity coefficient of component i in the liquid mixture and the fugacity coefficient of pure liquid compound i, respectively. Fugacity coefficients were obtained by knowing the residual chemical potential and compressibility factor.

3.2 | COSMO-RS model

The COSMO-RS model proposed first by Klamt,[53] as an *a priori* thermodynamic model that is independent of experimental data, has been widely used to predict the thermodynamic properties of systems containing ILs or DESs,[62–64] such as gas solubility, viscosity, vapor pressure, and activity coefficient. In this work, the COSMO-RS model as proposed was used to predict the VLE of the DES–toluene systems to validate the suitability of the model. The COSMO-RS calculation for VLE prediction was performed via the COSMOthermX19 code. Particularly, the corresponding COSMO files of HBAs and HBDs were prepared by geometry optimization and energy calculation COSMO solvation environment via Gaussian 09 software (Version D.01)[65] under the theoretical method of BP86/TZVP.[66,67]

3.3 | MD simulations

MD simulations carried out via the GROMACS (version 2019.1) software[68] were used to explore the microscopic interactions and particle distribution in the mixed systems at the bulk micro-molecular level. The simulated systems involved with pure toluene, DESs, and DES + toluene, and details of the simulated systems generated by PACKMOL tool[69] are given in Table S2. The molecular geometry structures simulated are shown in Figure 1. All molecules were described using the GAFF force fields generated by AmberTools18 software.[70] The atomic charges of all simulated molecules are obtained by using RESP method charges generated by the Multiwfn code,[71] based on geometrically optimized molecular structures generated by Gaussian 09 software at the B3LYP/6-311+G** level,[72] combining with DFT-D3 (BJ) dispersion correction.[73] Three-dimensional periodic boundary conditions were applied to all the simulated systems. The temperature control method is V-scaled and the pressure control methods are Berendsen barostat and Parrinello–Rahman. The electrostatic and van der Waals (vdW) interactions are described by the PME and cut-off

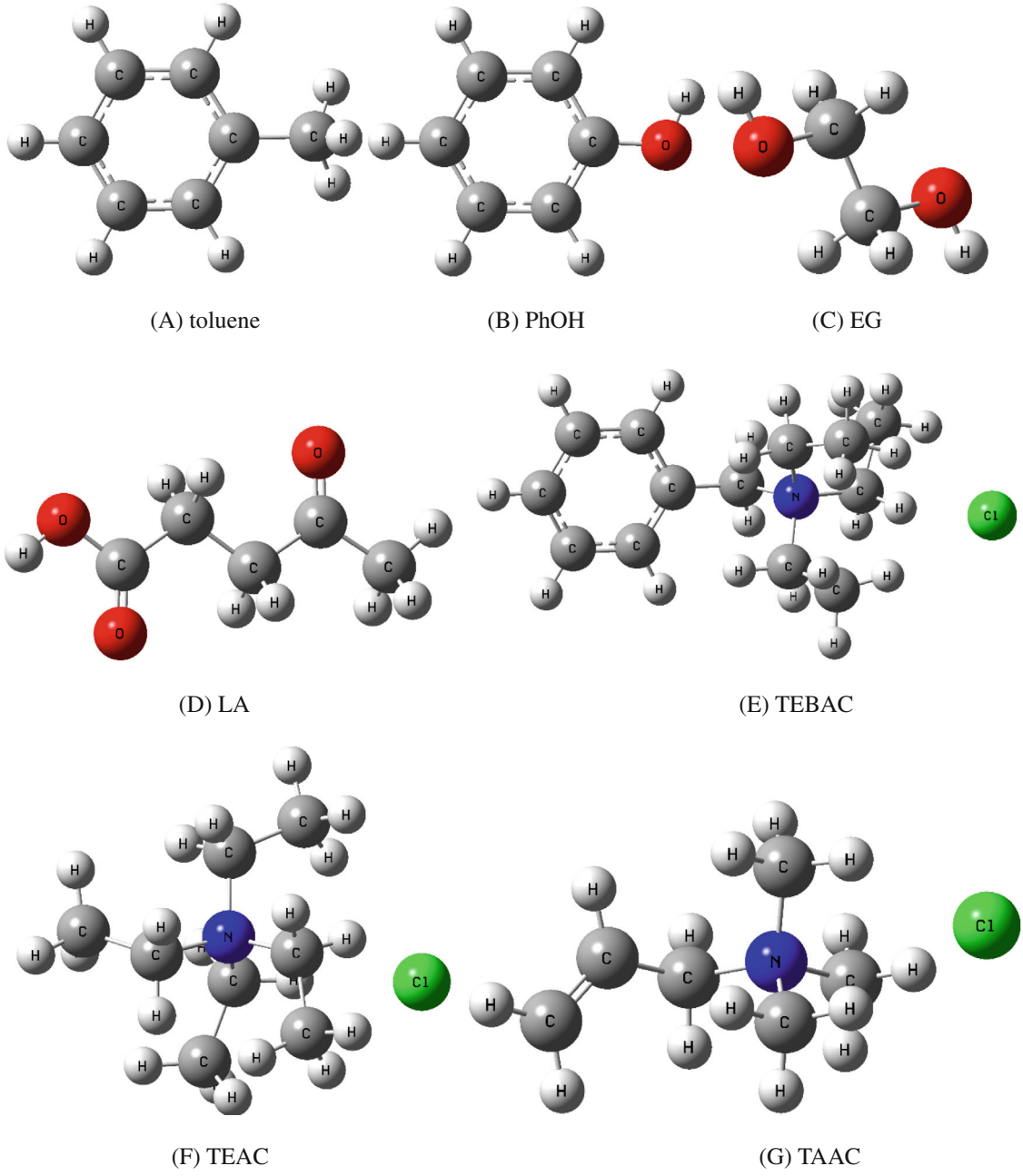

FIGURE 1 The molecular geometry structures of toluene, HBAs, and HBDs simulated this work.

methods, respectively, both of which have a cut-off distance of 1.2 nm. For each system, the simulation process consists of the following three steps. (i) The energy minimization is carried out. (ii) The equilibrium MD simulation is performed under the isothermal–isobaric ensemble (NPT) at 1 bar and 313.15 K for 10 ns, where the time step is 0.001 ps, using the Berendsen method to control the system pressure. (iii) The production MD simulations is conducted under NPT (1 bar and 313.15 K) using Parrinello–Rahman pressure control method lasting 50 ns. Eventually, the trajectory of the last 20 ns was collected for post-processing and analysis, such as atomic number density (AND) distributions and radial distribution functions (RDFs), spatial distribution functions (SDFs), interaction energy analysis, and diffusion coefficients. The reliability of the force field parameters used in this work was checked by comparing the calculated density of the simulated pure DES systems with the experimental data as shown in Table S3.

3.4 | Gibbs free energy of solvation

The magnitude of Gibbs free energy of solvation (ΔG_{sol}) of a gas molecule in solvents can reflect the absorption capacity of gas in solvents. In MD simulations, ΔG_{sol} of toluene in various DESs was produced based on the alchemical free energy calculation by constructing a

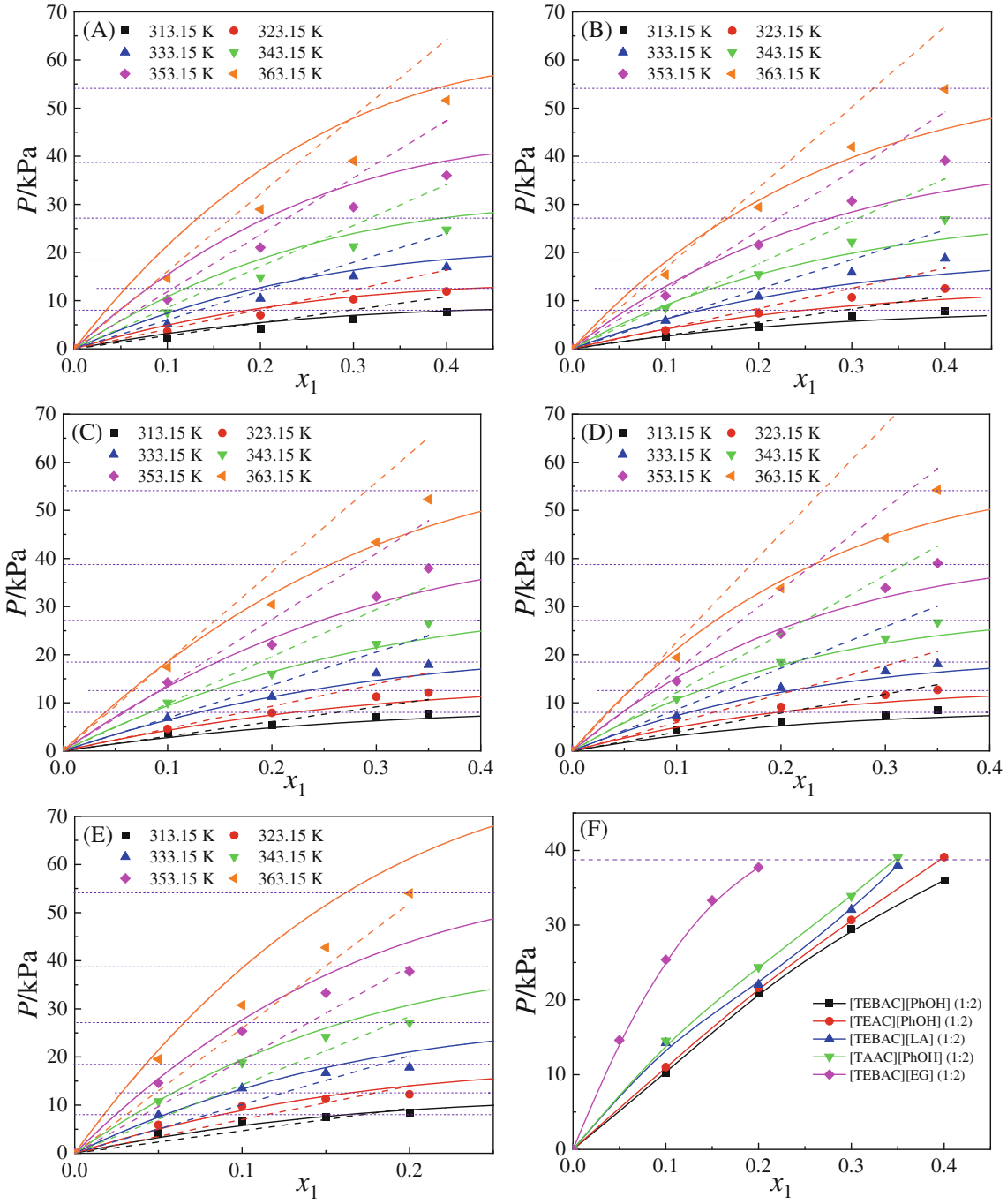

FIGURE 2 Vapor–liquid equilibrium (VLE) for toluene (1) in different DESs (2) (HBA:HBD = 1:2) of [TEBAC][PhOH] (A), [TEAC][PhOH] (B), [TEBAC][LA] (C), [TAAC][PhOH] (D), and [TEBAC][EG] (E) under various temperatures (Points, experimental data; solid lines, values predicted by the PC-SAFT model; dashed lines, values predicted by the COSMO-RS model; horizontal dotted lines, the pure toluene vapor pressure at the given temperature), as well as the experimental VLE comparison of toluene in different DESs at 353.15 K (F).

reversible thermodynamic path, which consists of a set of alchemical transition states connecting the initial (H_i: completely decoupled) and finally (H_f: completely interacting) states represented by

$$H(\lambda) = (1-\lambda)H_i + \lambda H_f \quad (8)$$

where H refers to the Hamiltonian, λ denotes a set of coupling parameters. The energy difference between a double of neighboring states was obtained by means of the Bennett acceptance ration (BAR) method in free energy perturbation methods.[74] Particularly, the intermolecular interaction between solutes and solvents is composed of Coulombic and Lennard–Jones items, are turned on individually. The Coulombic interaction was calculated by using a set of relatively large λ values (0, 0.2, 0.4, 0.6, 0.8, and 1) because of the relatively weak electrostatic interaction between toluene and DES molecules, and the Lennard–Jones interaction was described by the smaller λ values from

0 to 1 at an interval of 0.05 to ensure the simulation efficiency. In MD simulation for ΔG_{sol} calculation, all simulated boxes are embedded into 1 toluene and 100 HBA and 200 HBD molecules at 1 bar and a wide temperature range. First of all, the box was run for the energy minimization, and then was equilibrated at NVT and NPT ensembles for 10 and 100 ps, respectively, with a time step of 1 fs based on the Berendsen barostat. Finally, the production MD was run at the NPT ensemble using Parrinello–Rahman pressure control lasting for 8 ns, and related trajectories were used to collect data to further calculating ΔG_{sol}.

4 | RESULTS AND DISCUSSION

4.1 | VLE of DES + toluene systems

The VLE of five binary DES–toluene (HBA:HBD = 1:2) systems was experimentally measured and then predicted by PC-SAFT and COSMO-RS at the wide range of temperature (313.15–363.15 K) and toluene content (0–0.4 molar fraction), and the results are shown in Figure 2. The experimental VLE data and the values predicted by the PC-SAFT and the COSMO-RS models together in detail are summarized in Table S4. As expected, increasing temperature increases the system pressure for all DES–toluene systems, which indicates that high temperatures are harmful to the toluene absorption in DESs. Further, higher toluene content causes higher system pressures at isothermal conditions. Evidently, PC–SAFT provides an accurately quantitative prediction for all the DES–toluene systems with the total average relative deviations (ARDs) of 12.29%. Whereas, the COSMO-RS model can provide a qualitative and even semi-quantitative prediction with the total ARD of 24.12%. The details of deviations between experimental VLE data and values predicted by both COSMO-RS and PC-SAFT models are shown in Table S4. This completely demonstrates that the PC-SAFT is more suitable for describing the DES systems than the COSMO-RS model, which is ascribing to the fact that the strong HB interaction between HBAs and HBDs in DESs can be reasonably expressed by the association term (a^{assoc}) in original PC-SAFT equation. Meanwhile, the reason for the relatively large deviation of the COSMO-RS model may be that the corresponding parameters describing HB interactions were obtained by regressing the thermodynamic data of conventional organic solvents, resulting in the inconsistency for the systems containing DESs. In fact, the modeling accuracy of COSMO-RS model can be further improved by re-regressing adjustable parameters based on large amounts of experimental phase equilibrium data of mixed systems of DES–solute as stated by our previous work,[62] however, it is a big challenge to obtain abundant experimental data. Meanwhile, the modeling accuracy of PC-SAFT model can be also strengthen by adding the binary interaction parameter (i.e., $k_{ij} \neq 0$, $k_{ij} = 0$ in this work in order to the universal adaptability) by regressing the experimental VLE data of DES–toluene systems.

Further, the VLE behaviors of the different DES–toluene systems were compared at a given temperature (353.15 K), as shown in Figure 2F. An increasing order in system pressure of the DES–toluene mixtures was found: [TEBAC][PhOH] < [TEAC][PhOH] < [TEBAC][LA] < [TAAC][PhOH] < [TEBAC][EG]. This shows that lower pressure of binary DES–toluene systems is corresponding to a stronger absorption capacity of toluene for the counterpart DES. When considering the effect of different HBAs (i.e., TEBAC, TEAC, and TAAC) on the VLE of DES–toluene systems at the given HBD (PhOH), it is observed from Figure 2F that TEBAC causes the lowest DES–toluene system pressures among the three HBAs with the order of TEBAC < TEAC < TAAC, indicating that the HBA with the phenyl group can obviously decrease the system pressure of DES–toluene systems. Furthermore, the effect of different HBDs (EG, LA, and PhOH) on the VLE of DES–toluene systems was studied at the given HBA (TEBAC). Here, it can be observed that PhOH causes the lowest DES-toluene system pressure among the three HBDs, indicating that introducing phenyl (i.e., benzene ring in PhOH) into the HBD can obviously decrease the system pressure of DES–toluene systems. Therefore, the DES of both HBA and HBD with phenyl (i.e., [TEBAC][PhOH]) exhibits the smallest system pressure in relevant DES–toluene systems among all DESs studied in this work. This might result from the fact that the presence of phenyl group enables an enhanced intermolecular interaction of HBA/HBD–toluene. Moreover, the [TEBAC][PhOH] has the highest viscosity as an important absorption kinetics index among five DESs (Figure S2). In general, the more viscous absorbent is corresponding to the poorer mass transfer in the absorption process. In fact, the mass transfer problems can be overcome by designing and selecting efficient trays or packing in an absorption column in the real absorption unit process at the industrial scale. Therefore, we more focus on the thermodynamic absorption capacity of toluene in DESs in this work.

4.2 | Thermodynamic characteristics

4.2.1 | Henry's law constants

The Henry's law constant is one of the very significant thermodynamic properties to directly reflect the magnitude of solubility of a solute in a solvent. Moreover, the higher the Henry's law constant represents the lower solubility. Therefore, Henry's law constants of toluene in five DESs were calculated based on experimental data as shown in following relation

$$H_{1,2} \equiv \lim_{x_1 \to \infty} \frac{f_1}{x_1} \approx \frac{P_1}{x_1} \tag{9}$$

where f_1 and P_1 represent the fugacity and partial pressure of toluene in binary systems of toluene (1) + DES (2), x_1 refers to the molar fraction of toluene. It can be regarded as $f_1 = P_1$ due to the low system pressure. Henry's constants can be obtained by linear fitting the VLE data from Figure 2 based on Equation (1), as summarized in Table 2. It is observed that with the increase in temperatures, the Henry's constant is also increasing, indicating that the lower temperature helps DESs enhance the absorption capacity of toluene.

TABLE 2 Henry's law constants of toluene in different DESs, in kPa.

	$H_{1,2}$ (kPa)				
T/K	[TEBAC][PhOH]	[TEAC][PhOH]	[TEBAC][LA]	[TAAC][PhOH]	[TEBAC][EG]
313.15	19.25	21.32	24.22	26.19	49.25
323.15	30.24	33.55	36.86	39.82	72.25
333.15	46.39	50.08	53.56	55.77	104.27
343.15	66.72	71.15	76.87	80.56	152.99
353.15	94.91	100.90	109.51	114.86	210.79
363.15	132.07	138.61	149.46	156.06	283.61

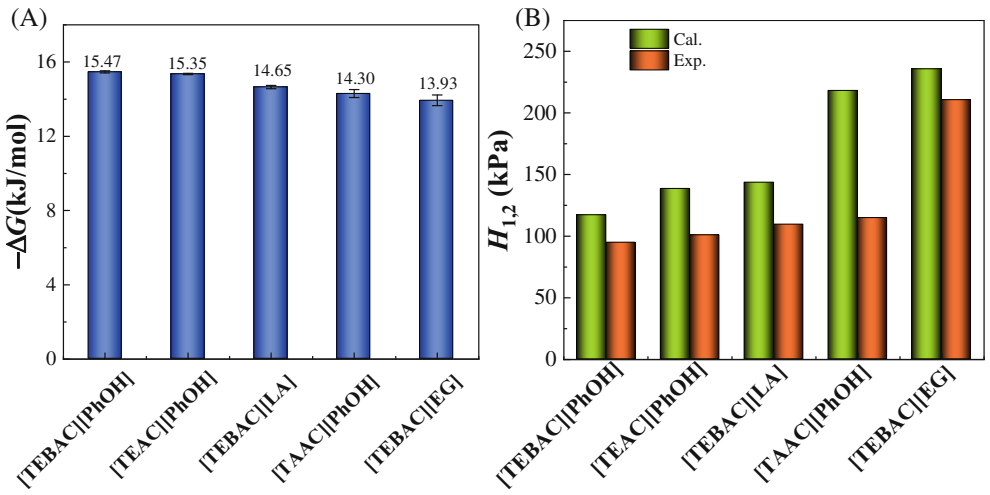

FIGURE 3 The calculated free energy of solvation (ΔG_{sol}) of toluene by MD simulations (A), and the comparison of calculated and experimental Henry's law constants of toluene (B) in five DESs (HBA:HBD = 1:2) at 353 K.

4.3 | Excess enthalpy of toluene in DESs

In addition, the enthalpy change (ΔH) in absorption process can be calculated based on the experimental Henry's constant by the following equation[75]

$$\partial \ln H_{1,2} = -\frac{\Delta H}{R}\partial\left(\frac{1}{T}\right) \tag{10}$$

where T and R represent the temperature and ideal gas constant, respectively. In this case, ΔH can be readily obtained by linear fitting of $\ln H_{1,2}$ and $1/T$. As shown in Figure S7, the strong linear relationship between $\ln H_{1,2}$ and $1/T$ is presented in all the DES–toluene systems. All the DES–toluene systems have the negative ΔH (Figure S7F), indicating that the toluene absorption is an exothermic process. The magnitude of $|\Delta H|$ values follows the order of [TEBAC][PhOH] > [TEAC][PhOH] > [TEBAC][LA] > [TAAC][PhOH] > [TEBAC][EG]. Moreover, the [TEBAC][PhOH] demonstrates the most negative ΔH (-36.32 kJ·mol^{-1}), which indicates that the DES most easily absorb toluene among all counterparts. This is probably resulted from the strongest intermolecular interaction of TEBAC/PhOH–toluene.

4.4 | Gibbs free energy of solvation

The Gibbs free energy of solvation (ΔG_{sol}) values of toluene in different DESs (HBA:HBD = 1:2) obtained by the MD simulation are shown in Figure 3A. It is worth noting that the more negative ΔG_{sol} is, the stronger solvation performance of toluene in DESs is, which benefits the toluene absorption process. For the same HBA (i.e., TEBAC), ΔG_{sol} magnitude exhibits a significantly increasing negative trend with the order of PhOH < LA < EG, indicating that the DES of the HBD with phenyl is favorable to the toluene solvation. For the same HBD (i.e., PhOH), ΔG_{sol} magnitude follows the order of TEBAC > TEAC > TAAC at different HBAs, similarly, DES of HBA with phenyl is favorable to the toluene solvation. Thus, the DES [TEBAC][PhOH] demonstrates the most negative ΔG_{sol} value. It is worth noting that the Henry's law constant $H_{1,2}$ can be obtained by ΔG_{sol} as shown below

$$H_{1,2} = \frac{\rho RT}{M}\exp\left(\frac{\Delta G_{sol}}{RT}\right) \tag{11}$$

where ρ and M denote to the density and molecular weight of DESs (HBA:HBD = 1:2), respectively; R and T represent the ideal gas constant (8.314 J·mol^{-1}·K^{-1}) and the temperature of systems. The Henry's law constants based on ΔG_{sol} are illustrated in Figure 3B. When compared with the experimental Henry's law constant, the results calculated by using ΔG_{sol} has a good consistency, further indicating the reliability of MD simulations. Although a relatively large deviation appears at the [TACC][PhOH] system, there is the qualitative consistency between the experimental and simulated results. The largest deviation is presented in [TACC][PhOH] among all DESs studied in this work, which does not demonstrate the specificity, but is only a general problem based on the MD simulation. Of course, we

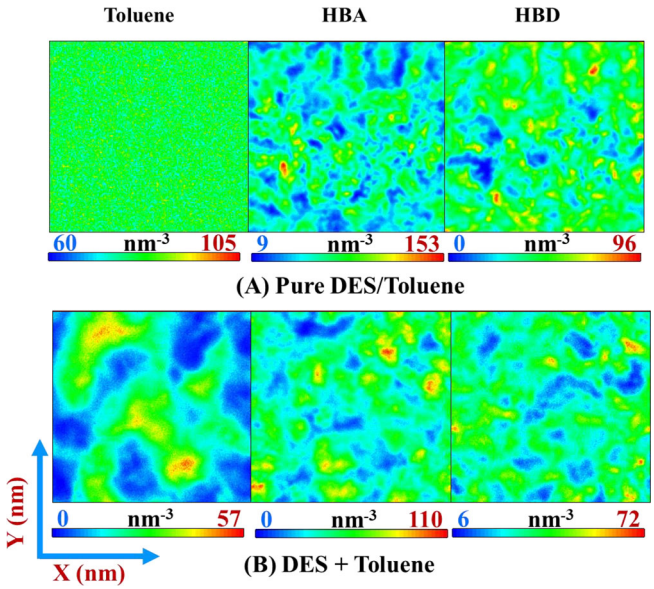

FIGURE 4 Atom number density (AND) distributions of toluene, HBA, and HBD observed along the $x-y$ plane in pure toluene/DES ([TEBAC][PhOH] (1:2)) (A), and DES–toluene systems (B).

believe that the accuracy of the calculation can be further improved by the following three options: (i) reducing the step of electrostatic interaction during the free energy calculation; (ii) increasing the number of DES molecules in the simulated system during the free energy calculation, in order to be closer to the infinite dilution condition and to further describe the real Henry's law constant more accurately; (iii) improving the force field parameters of toluene, DES molecules (e.g., Lennard–Jones potential parameters, bonds, angles, and dihedral angles). The more negative ΔG_{sol} value of the DES is, the lower the Henry's law constant is. The similar conclusion with ΔG_{sol} is also presented in Henry's law constant results, that is, the Henry's law constant for the DES consisting of both HBD and HBA with phenyl (i.e., [TEBAC][PhOH]) has the lowest values among all the DESs studied in this work. Thus, the [TEBAC][PhOH] is a preferred candidate DES for toluene absorption process. If we want to design and develop a more efficient DES to enhance the toluene absorption capacity, the HBAs and HBDs with the more phenyl group should be considered. From the structure–property relationship perspectives, the difference between ΔG_{sol} and Henry's law constants of toluene in various DESs is fundamentally due to the structural factors of HBAs and HBDs, which will be further discussed as follows.

4.5 | Atom number density distributions

The microscopic mixing behavior at the atomic scale based on the bulk micro-molecular level derived from the MD simulation can be directly visualized by observing the atom number density (AND) distributions (observed along the x–y plane). Figure 4 shows the color-filled maps of AND distributions for pure toluene, DES ([TEBAC][PhOH] (1:2)), and DES–toluene systems. It can be seen from Figure 4A that pure toluene demonstrates the highly homogeneous or isotropic behavior due to the extremely small size of density distribution regions. However, the AND for the DES system exhibits the inhomogeneous or anisotropic distribution behavior of both HBD and HBA, indicating the mixing phenomenon dominated by the HB interaction between HBD and HBA. For the DES–toluene systems (Figure 4B), the AND homogeneity of toluene is significantly changed into the aggregated distribution with strong anisotropy in the presence of the DES molecule. This is because of the stronger interaction is formed between DES and toluene, which destroys the original interaction between toluene molecules. This is the reason that adding DES into toluene can significantly decrease the vapor pressure (Figure 2). Similarly, the AND distributions of HBD and HBA in the DES–toluene system are more anisotropic than those in a single DES system, due to the HB network between HBD and HBA affected by the toluene. The analogous phenomena are also presented in other pure DESs and DES–toluene systems as shown in Figures S8–S11. In short, the above findings further understand the VLE behavior of DES–toluene systems and toluene absorption process from the perspective of microscopic distribution of bulk molecule, which is accordant with the VLE experimental results. In principle, the microscopic distribution of bulk molecule is resulted from the intermolecular interaction toluene–toluene and HBD–/HBA–toluene as mentioned below.

4.6 | Structural distribution and intermolecular interaction of bulk molecules

The microscopic structural distribution and intermolecular interaction for these DES–toluene is further recognized by the radial distribution function (RDF) analyses, referring to probability distribution of counted atoms or positions around a central reference position or atom. The RDF profiles for different DES–toluene systems are given in Figure 5. It can be seen from Figure 5A that when compared with the RDF profile of center of mass (COM) of toluene–toluene in pure toluene system, the first sharp peak presented at about $r = 0.60$ nm demonstrates the higher strength in DES–toluene systems, indicating that the association between toluene–toluene (or interaction between molecules) affected by the presence of the DES. Evidently, there is the different intensity of the peak for distinct DES–toluene systems, the higher peak is corresponding to the more concentrated distribution of toluene to form the toluene cluster. These findings are consistent with the AND distribution results (Figure 4). The structural distribution and intermolecular interaction between different HBDs (PhOH, LA, and EG) and toluene can be described by the RDF between hydrogen (H_{OH}) on hydroxyl of HBDs and COM of toluene as shown in Figure 4B. It is found that the intensity of interaction of HBD–toluene is in the order of PhOH > LA > EG under the same HBA due to the same trend of the position of the first peak. This is consistent with the experimental results, that is the PhOH with phenyl has the stronger interaction with toluene resulting in the lower system pressure of DES–toluene systems (Figure 2).

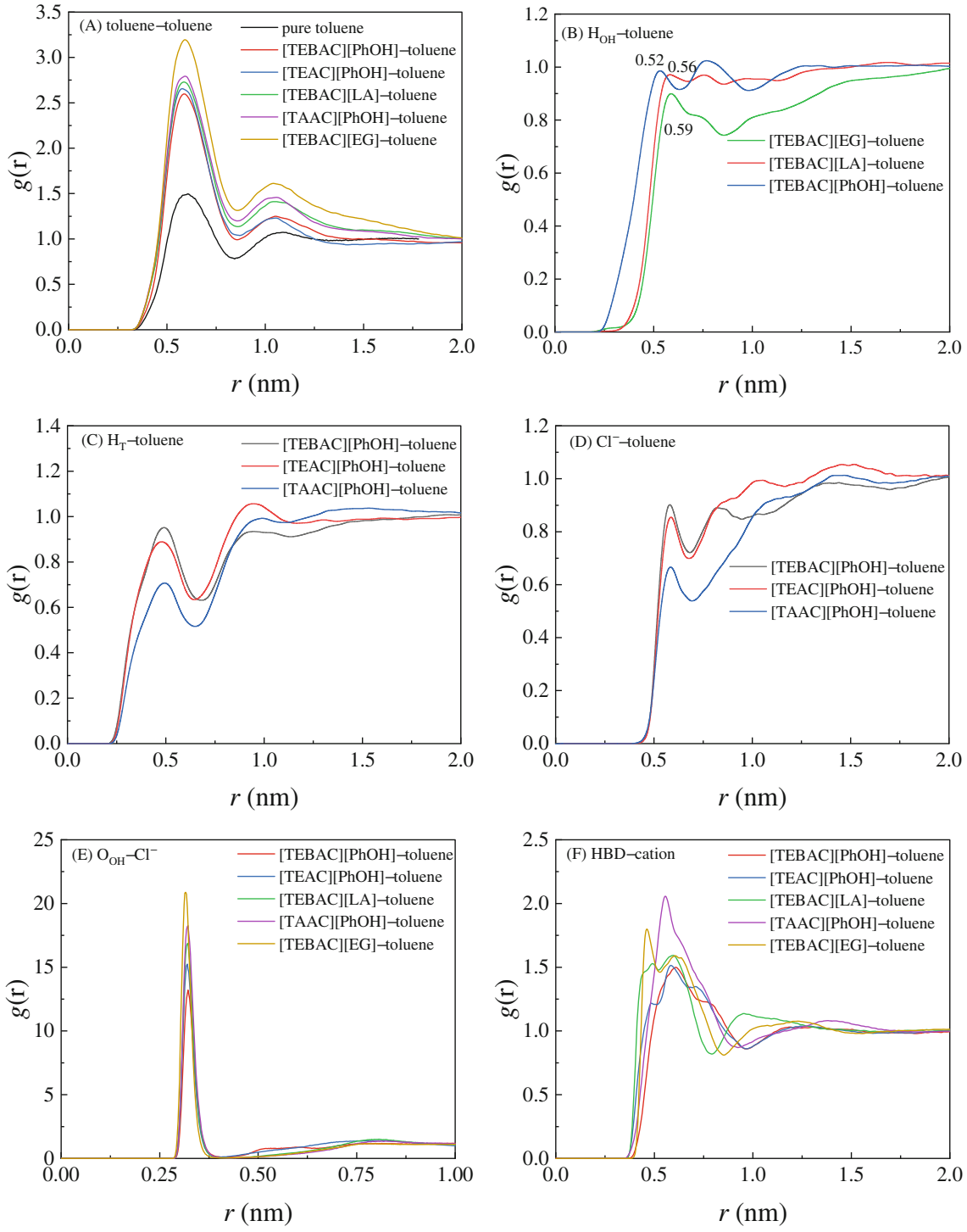

FIGURE 5 Radial distribution functions (RDFs) for center of mass (COM) of toluene–toluene (A) H_{OH}–COM of toluene (B), H_T–COM of toluene (C), Cl^-–COM of toluene, and (D) for different DES–toluene systems (HBA:HBD = 1:2).

The effect of HBAs on the structural distribution and intermolecular interaction of HBA–toluene is shown in Figure 5C,D. It can be seen from Figure 5C that the RDF of terminal hydrogen (H_T) of alkyl chain in HBA and COM of toluene under the same HBD shows the first peak at around r = 0.50 nm, representing the formation of C–H···π interaction between alkyl chain of HBA and toluene according to the previous research findings.[50] The RDF between Cl^- and COM of toluene shows that the first peak of the three DES–toluene systems appear at about r = 0.55 nm (Figure 5D), indicating the π···H···Cl^- interaction of TEBAC–toluene. Especially, TEBAC has the strongest association with toluene because of the highest RDF peaks of both H_T–toluene and Cl^-–toluene presented in the [TEBAC][PhOH]–toluene system. Figure 5E,F shows the distribution and interaction of HBA–HBD. The HBD interacts with both the Cl^- and the

TABLE 3 Interaction energies including van der Waals energy, electrostatic energy, and total energy of HBA−/HBD−/DES−toluene in five DES−toluene (HBA:HBD = 1:2) systems, in kJ/mol (error bar values shown in brackets).

Types of DES	HBA−toluene			HBD−toluene			DES−toluene		
	E_{vdW}	E_{Ele}	E_{Total}	E_{vdW}	E_{Ele}	E_{Total}	E_{vdW}	E_{Ele}	E_{Total}
[TEBAC][PhOH] (DES1)	−26.21 (±0.88)	−4.17 (±0.08)	−30.38 (±0.90)	−25.98 (±0.85)	−2.77 (±0.06)	−28.75 (±0.93)	−52.19 (±1.13)	−6.95 (±0.05)	−59.14 (±1.33)
[TEAC][PhOH] (DES2)	−23.13 (±0.55)	−4.74 (±0.09)	−27.88 (±0.67)	−24.86 (±0.46)	−2.29 (±0.05)	−27.15 (±0.84)	−48.00 (±0.85)	−7.03 (±0.06)	−55.03 (±0.95)
[TEBAC][LA] (DES3)	−21.73 (±0.57)	−4.74 (±0.04)	−26.47 (±0.89)	−22.82 (±0.67)	−1.62 (±0.05)	−24.44 (±1.06)	−44.54 (±1.26)	−6.36 (±0.03)	−50.9 (±1.11)
[TAAC][PhOH] (DES4)	−16.45 (±0.45)	−4.99 (±0.06)	−21.44 (±1.02)	−20.61 (±0.68)	−1.39 (±0.07)	−22.01 (±0.76)	−37.06 (±1.06)	−6.38 (±0.006)	−43.44 (±1.21)
[TEBAC][EG] (DES5)	−14.69 (±0.38)	−4.05 (±0.08)	−18.74 (±0.45)	−16.01 (±0.49)	−1.03 (±0.10)	−17.03 (±0.77)	−30.7 (±0.97)	−5.07 (±0.08)	−35.78 (±0.89)

cation in the HBA, and the strong HB force dominates the HBD–Cl^- interaction represented by the sharp peak (about $r = 0.31$ nm) for the RDF of oxygen (O_{OH}) on hydroxyl of HBDs and Cl^-. Both interaction of HBD–cation and HBD–Cl^- follow the order of [TEBAC][PhOH] > [TEAC][PhOH] > [TEBAC][LA] > [TAAC][PhOH] > [TEBAC][EG]. This is because that the stronger interaction of HBA–HBD, which is the exact opposite of the order of experimental vapor pressure. It is because of there is a competitive effect presented in the HBA−/HBD–toluene and HBA–HBD, and the stronger interaction of HBA–HBD is corresponding to the weaker counterpart of HBA−/HBD–toluene.

4.7 | Interaction energy analysis

To quantitatively explore the reason for the difference in VLE behavior of toluene in 4–5 DESs ILs and understand the interaction mechanism between DES (HBA/HBD) and toluene, investigating the intermolecular interaction energy at bulk molecular level is of great significance. It should be noted that the interaction energy consists of vdW and electrostatic (Ele) interactions in MD simulations. In this work, the respective contributions of vdW and Ele interactions to the total interaction between DES (HBA/HBD) and toluene can be clearly identified. The calculated results are presented in Table 3 and Figure 6 (see Supporting Information for more details on interaction energy calculation, which can be also found in Huang et al.'s work.[76]). It can be seen from Table 3 that the interaction energies between DESs and toluene have a consistent correlation with the VLE experimental results, that is, the larger interaction energy corresponds to the lower vapor pressure of DES–toluene systems. The vdW interaction of DES–toluene is almost an order of magnitude higher than the electrostatic interaction of counterpart, indicating the former will play an dominate role in VLE behaviors and potential VOC absorption with DESs. Figure 6A shows that both the HBA and HBD play the comparable role in DES–toluene systems due to the small difference in interaction energies between HBA–toluene and HBD–toluene, in which the vdW plays a decisive role. For the interaction of HBA–toluene, it can be divided into the sum of cation and anion (Cl^-) with toluene. Figure 6B shows that the vdW attraction interaction of cation–toluene has the dominate contribution to the total interaction of HBA–toluene. The Ele attraction dominates the interaction of Cl^-–toluene. The Ele repulsion of cation–toluene between the Ele attraction of Cl^-–toluene cancels each other out resulting in the negligible contribution of Ele interaction of HBA–toluene to total interaction of that (Figure 6A). Figure 6C,D shows that the size order for interaction of HBA (cation/Cl^-)–HBD, which is dominated by the Ele interaction of Cl^-–HBD, is opposite to that of DES (HBA/HBD)–toluene in five DESs. This is because of the DES with the stronger HB interaction of HBA–HBD has the relatively fixed position resulting in the decrease of free movement opportunity to contact with the toluene molecule, which lead to the weaker interaction of HBA−/HBD–toluene. The interaction energy of HBA–HBD is significantly and even an order of magnitude higher than that of DES–toluene, which is the evident of DES

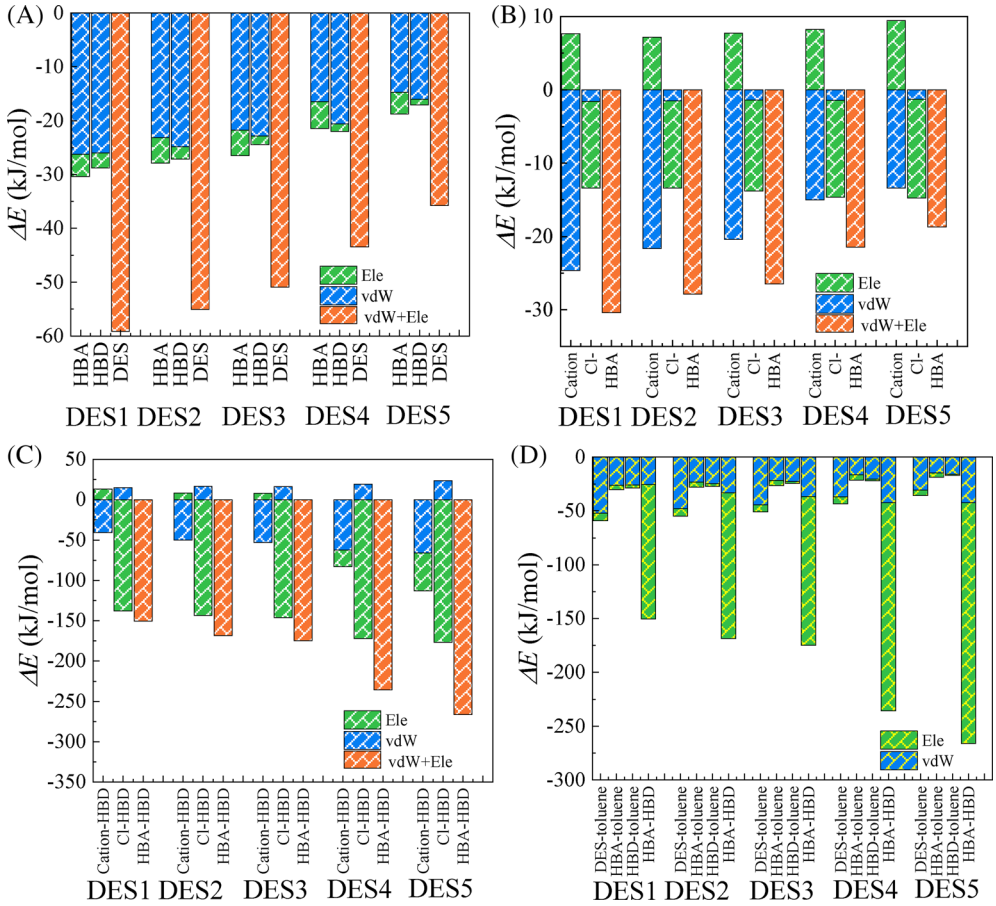

FIGURE 6 Interaction energies of HBA–/HBD–/DES–toluene (A), interaction energies cation–/Cl^-–/HBA–toluene (B), cation–/Cl^-–/HBA–HBD (C), and comparison for E_{vdW} and E_{Ele} of HBA–/HBD–/DES–toluene and HBA–HBD and in five DES–toluene (HBA:HBD = 1:2) systems.

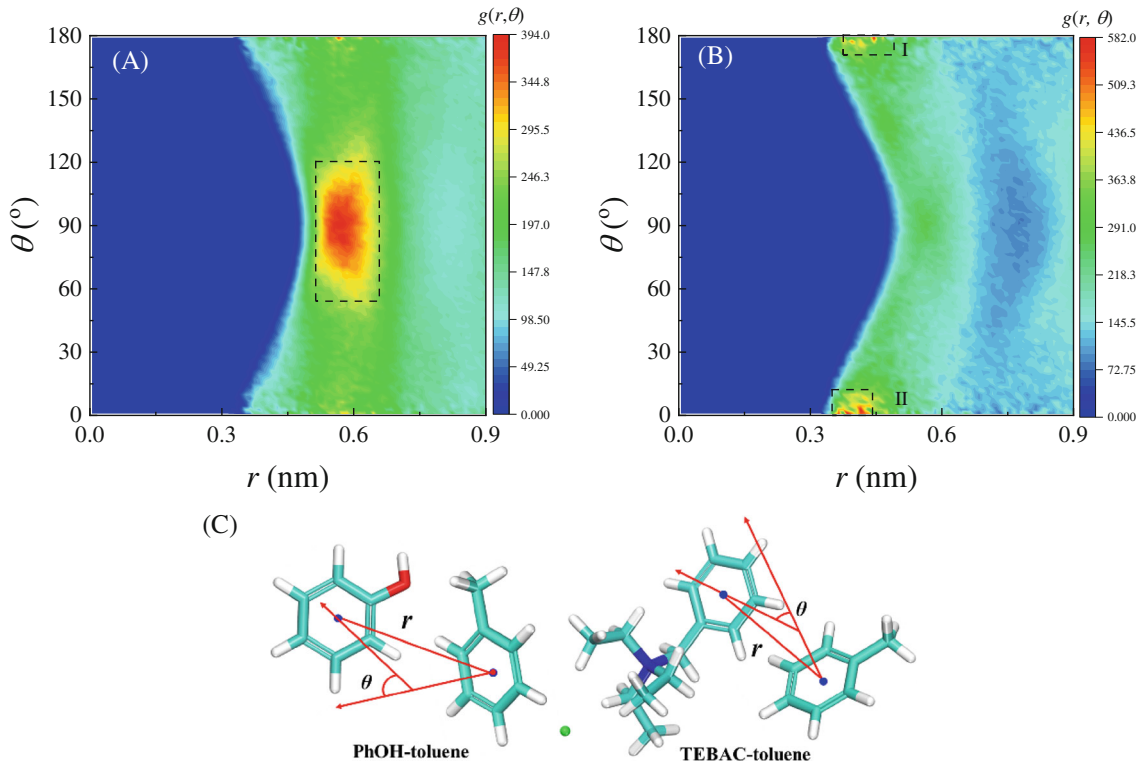

FIGURE 7 Angular and distance distributions (ADDs) of two benzene ring planes in PhOH–toluene (A) and TEBAC–toluene (B) systems, and the schematic illustration of relationship between θ and r (C).

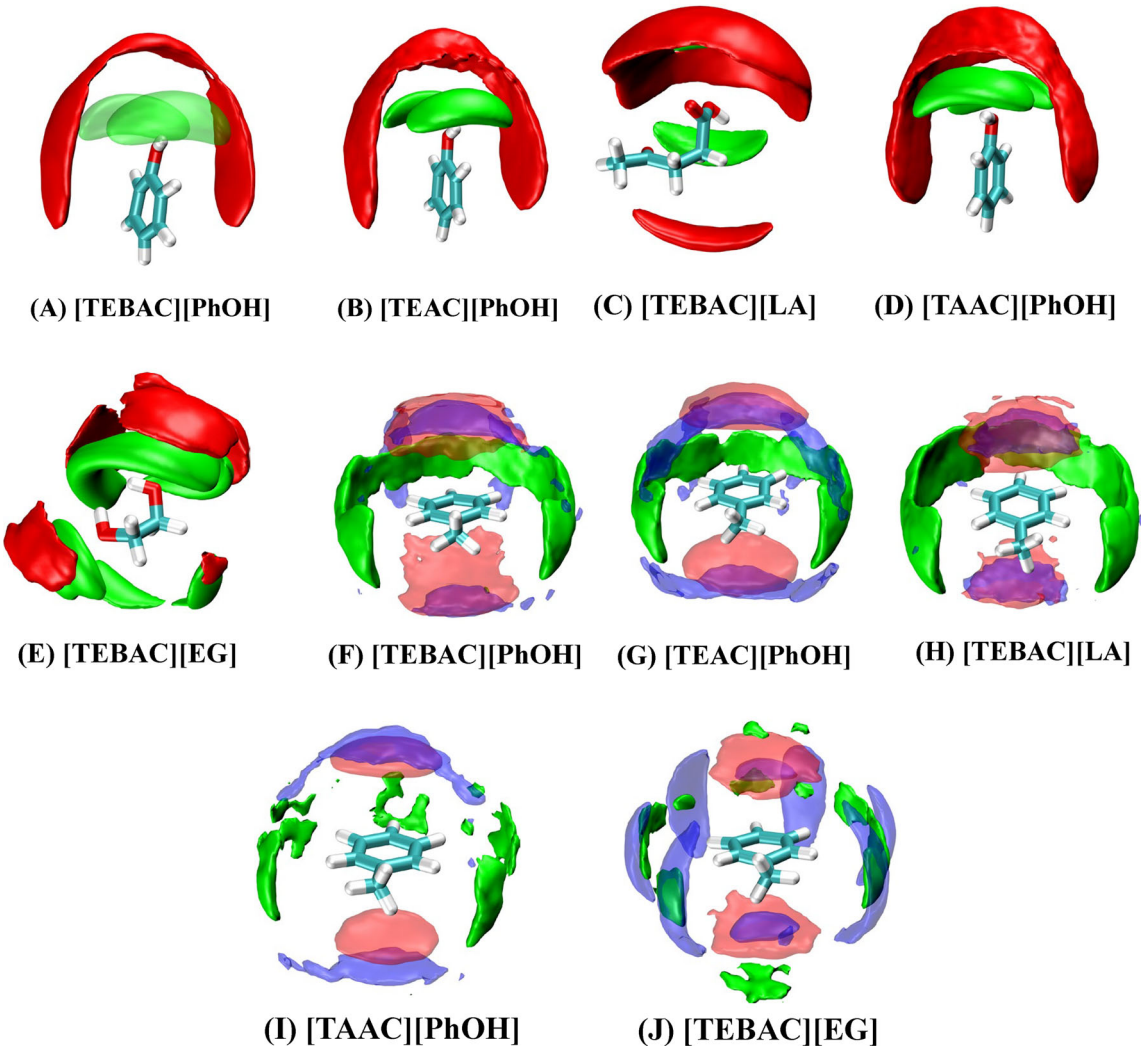

FIGURE 8 Spatial distribution functions (SDFs) of cations (red) and Cl^- (green) on HBAs around HBDs (A–E), as well as HBDs (blue) and cations (red) and Cl^- (green) of HBAs around toluene (F–J) in five DES–toluene (HBA:HBD = 1:2) systems.

formation by means of strong HB interaction. Anyway, it can be confirmed that the interaction energy analysis is in accordance with the VLE experimental results, Henry's law coefficients, excess enthalpies, and ΔG_{sol}, and RDF analyses, that is, the DES consisting of both HBD and HBD with phenyl has the best toluene absorption capacity, the lowest vapor pressure of DES–toluene system, and strongest interaction of DES–toluene among five DESs studied in this work.

4.8 | Identifying π–π interaction of bulk molecules

In order to explore whether the π–π interaction can be formed between toluene and phenyl on DESs, the angular and distance distributions (ADD, g(*r*,*a*)) between benzene rings of DES and toluene were analyzed by determining the distance (*r*) between COMs of two benzene rings and angle (*θ*) between two normal vectors to benzene rings as shown in Figure 7. The ADD is defined as the following equation[77]

$$g(r,\theta) = \frac{Vn(r,\theta)}{N4\pi^2\Delta r} \quad (12)$$

where $n(r, \theta)$ represents the number of molecules under r and θ, V and N represent the bulk volume and the number of bulk molecules, respectively. For the PhOH–toluene (Figure 7A), it is found that there is the highest density region distributed in 0.50 nm < r < 0.65 nm with an about 90° angle, indicating that the T-shaped perpendicular orientation distribution presented between two benzene rings to further confirm the formation of π···H···π interaction. For the TEBAC–toluene (Figure 7B), there are two high density regions (sections I and II) distributed in the 0° < θ < 20° and 170° < θ < 180° combining with 0.35 nm < r < 0.50 nm, indicating that the two benzene rings of both TEBAC and toluene is mainly presented the parallel distribution dominated by the π–π stacking.[78] The above findings are consistent with the AND distributions, RDF, and interaction energy analyses and further complement the identification of microscopic mechanism for the

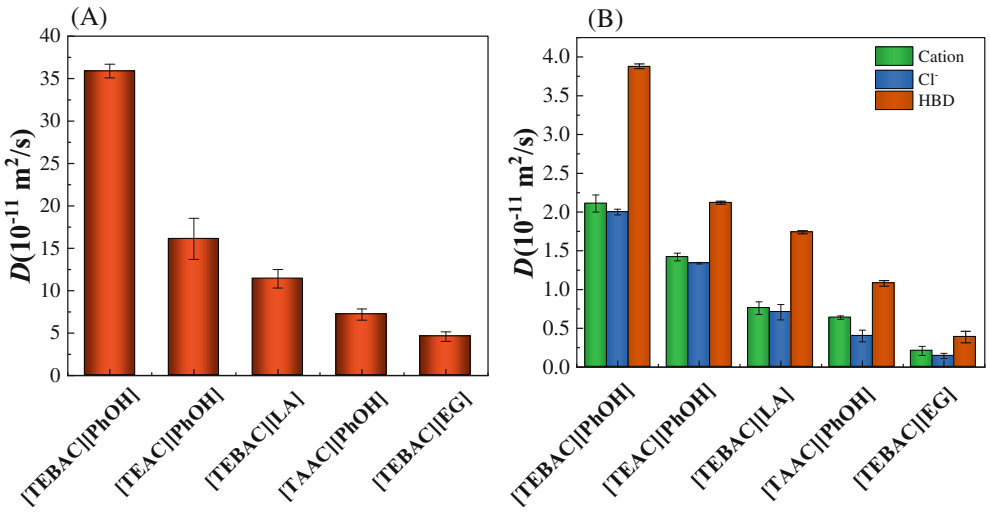

FIGURE 9 Self-diffusion coefficients (*D*) of toluene (A), cation and Cl^- on HBAs, and HBDs (B) in five DES–toluene (HBA:HBD = 1:2) systems.

DES consisting of both the HBA and HBD with phenyl enhancing the absorption capacity of toluene with weak π–π-based interactions (e.g., π···H···π interaction and π–π stacking) between phenyl and toluene based on the bulk micro-molecular level.

4.9 | SDFs analysis

The SDFs were analyzed to visually observe the three-dimensional spatial distributions of other molecules/atoms around the specifically central molecule. The SDF analyses of five DES–toluene systems are illustrated in Figure 8. Figure 8A–E shows the spatial distributions of cations (red) and Cl^- (green) on HBAs around HBDs (i.e., PhOH, EG, and LA). It is found that the Cl^- is located around the hydroxyl of HBDs ascribed to the formation of HB interaction, and the cations appear farther around the HBD than the anions, wrapping the HBD in a larger area resulted from the larger volume of cation and vdW interaction of HBD–cation (see Figure 3). For the same HBD (i.e., PhOH), the area of free (unoccupied) space consisted of HBA and HBD follows the order of [TEBAC][PhOH] > [TEAC][PhOH] > [TAAC][PhOH] which is consistent with the interaction magnitude of HBA–HBD and the HBA molecule size. For the same HBA (i.e., TEAC), the decreasing order for area of free space consisted of HBA and HBD follows [TEBAC][PhOH] > [TEAC][LA] > [TAAC][EG] which is also consistent with the interaction magnitude of HBA–HBD. Figure 8F–J shows that the spatial distributions of HBDs (blue) and cations (red) and Cl^- (green) on HBAs around toluene. It can be seen that the most areas of HBD and full areas of cations of HBAs are distributed directly below and above the plane of the benzene ring of the toluene molecule, which is ascribed to these region focuses on the high π-electron cloud density, resulting in the formation of π–π-based interaction with cations and HBDs. Moreover, these areas follow the decreasing order of [TEBAC][PhOH] > [TEAC][PhOH] > [TEAC][LA] > [TAAC][PhOH] [TEAC][EG], indicating decreasing order of interaction between HBD/HBA and toluene. The Cl^- is relatively far distributed around the hydrogen atoms of toluene, which represents the formation of weak electrostatic interaction between toluene and Cl^-. The finding mentioned above is consistent with the RDF, interaction energy, and AND analyses.

4.10 | Self-diffusion coefficients

The dynamic property is the other significant index to evaluate the absorption process other than the thermodynamic behaviors such as absorption capacity and phase equilibrium behavior. The magnitude of diffusion coefficient of toluene in DESs can evaluate the dynamic priority of candidate absorbents. It can be confirmed that the ideal absorbent should simultaneously equip with both high absorption capacity and high diffusion coefficient of solute. Thus, self-diffusion coefficients (*D*) of toluene, HBAs, and HBDs in DES–toluene systems were calculated by using Einstein equation based on MD simulations as follows.

$$D_i = \frac{1}{6}\lim_{t\to\infty}\frac{d}{dt}\left\langle |r_i(t) - r_i(0)|^2 \right\rangle = \frac{1}{6}\lim_{t\to\infty}\frac{d\Delta r_i^2}{dt} \tag{13}$$

where $\left\langle |r_i(t) - r_i(0)|^2 \right\rangle$ represents the average mean square displacement (MSD) of the molecule *i*, and $r_i(0)$ and $r_i(t)$ refer to the vector coordinate of molecules at 0 and *t* time, respectively. It can be seen from Figure 9A, the diffusion coefficient of toluene in all of the DES–toluene systems follows the order of [TEBAC][PhOH] (1:2) > [TEAC][PhOH] (1:2) > [TEBAC][LA] (1:2) > [TAAC][PhOH] (1:2) > [TEBAC][EG] (1:2), which is reverse with the experimental results for VLE of DES–toluene systems. That is, the DES with the greater diffusion coefficient of toluene is corresponding to the system with the lowest system pressure of the VLE DES–toluene. This is in contrast to the phenomenon of the IL–H_2O system presented in our previous study,[79] that is, the IL with the greater diffusion coefficient of H_2O was corresponding to the system with the lowest system pressure of the VLE IL–H_2O. The reason is that the IL–H_2O system is dominated by the strong HB interaction of IL–H_2O, which leads to the strong

binding of H_2O molecules around IL molecules. In addition, the H_2O molecules are relatively small, and the free volume effect can be ignored, thus leading to the above corresponding phenomenon. However, the relatively weak vdW and π–π interaction of DES–toluene plays a leading role in DES–toluene systems, and the free volume effect of toluene in DES is highlighted due to larger size of the toluene molecule. Therefore, the DES with stronger interaction with toluene corresponds to weaker HB interaction of HBA–HBD, which leads to a larger free volume in DESs, resulting in more holes in the HBA–HBD HB network in the DES systems, which favors the local free movement of toluene molecules and further leads to a larger diffusion coefficient of toluene. Figure 9B shows that the diffusion coefficients of cation, Cl^- on HBAs and HBDs with the order of [TEBAC][PhOH] (1:2) > [TEAC][PhOH] (1:2) > [TEBAC][LA] (1:2) > [TAAC][PhOH] (1:2) > [TEBAC][EG] (1:2), have a same trend with that of toluene, but the former is an order of magnitude of the latter ascribed to the fact that the HB interaction of HBA–HBD is significantly stronger than vdW interaction of DES–toluene, hindering the free movement of HBA and HBD. Among the diffusion coefficients of cation, Cl^- on HBAs and HBDs, the diffusion coefficients of HBDs are significantly higher than that of cation and Cl^-, and there is almost the similar value presented between cation and Cl^- due to the greatly strong electrostatic interaction of cation–Cl^-. Anyway, the diffusion coefficients show the consistent phenomenon with the RDFs analysis and interaction energy calculations. This is further confirmed that a synergistic effect occurs between the thermodynamic behavior and dynamic diffusion in DES–toluene systems. Thus, the DES consisting of both the HBA and HBD with phenyl ([TEBAC][PhOH]) can be treated as the optimal absorbent for efficient toluene absorption.

5 | CONCLUSIONS

In our work, we systematically studied the structural effect on a series of phenyl-based DESs with (i.e., HBAs TEBAC, TEAC, or TAAC, and HBDs PhOH, LA, or EG) suitability as absorbents for toluene absorption from molecular thermodynamic and dynamic insights by VLE experiments and MD simulations. The VLE of binary DES–toluene systems were measured experimentally and predicted by PC-SAFT and COMSO-RS. The results demonstrated that the system pressure follows the order [TEBAC][PhOH] < [TEAC][PhOH] < [TEBAC][LA] < [TAAC][PhOH] < [TEBAC][EG] for the investigated DES–toluene systems, in which the DES consisting of the HBA and HBD with phenol ([TEBAC][PhOH]) has the lowest system pressure among all systems. PC-SAFT and COSMO-RS were used for modeling the VLE of DES–toluene systems, and both models provided quantitative predictions, while only PC-SAFT predictions were accurate. The thermodynamic analyses (i.e., Henry's constant, excess enthalpy of toluene, and ΔG_{sol} of toluene in DESs) are in accordance with the experimental VLE results. That is, the DES [TEBAC][PhOH] has the most negative excess enthalpy, most negative free energy of solvation of toluene, and the lowest Henry's law coefficient among all DESs. The molecular insights into the relationship between DES structures and thermodynamic behaviors of DES–toluene systems were deeply investigated by analyzing AND distributions, RDFs, SDFs, and interaction energy based on MD simulations. It can be confirmed that both HBAs and HBDs contribute to the interaction of DES–toluene, and the interactions of both HBA–toluene and HBD–toluene are dominated by the vdW interaction and the π–π-based weak interaction, as well as the almost negligible electrostatic interaction of DES–toluene is derived from Cl^-–toluene. In addition, for the DES–toluene with the same HBA (TEBAC), the interaction of HBD–toluene was in the order of PhOH–toluene > LA–toluene > EG–toluene, while for the same HBD (PhOH), the interaction of HBA–toluene follows the order of TEBAC–toluene > TEAC–toluene > TAAC–toluene. Thus, the DES (i.e., [TEBAC][PhOH]) simultaneously demonstrates the strongest interactions of HBA–toluene, and HBD–toluene was ascribed to the fact that the phenyl of [TEBAC] and [PhOH] leads to increase the additional π–π-based weak interaction between phenyl and toluene, and further result in the lowest vapor pressure of the [TEBAC][PhOH]–toluene system among all DESs. The dynamic diffusion behavior demonstrated that the magnitude of the diffusion coefficient of toluene in DES–toluene systems is consistent with that of interaction of DES–toluene, indicating a synergistic effect between the interaction and diffusion, that is, the DES with stronger interaction of DES–toluene corresponds to the higher diffusion coefficient of toluene. This is because the DES with stronger interaction of DES–toluene is corresponding to the relatively weaker electrostatic interaction of HBA–HBD. This results in a larger free volume space as well as cavities available for the free movement of toluene molecules presented in the DES system, leading to the larger diffusion coefficient. All in all, the DES [TEBAC][PhOH] consisting of both HBA and HBD with phenyl can be treated as an optimal absorbent based on its both the attracting thermodynamic behaviors and the high dynamic diffusion for toluene absorption among DESs studied in this work.

This work aims to provide theoretical guidance for rational design of novel DESs for the highly efficient aromatic VOCs absorption from the viewpoints of both the molecular thermodynamic behaviors and dynamic diffusion. Evidently, the findings and conclusion proposed in this study based on experiments, theoretical calculations, modeling, and simulations can be expected to directly guide the development of task-specific DESs for other VOCs absorption, and facilitates DES industrial applications in gas separation.

AUTHOR CONTRIBUTIONS

Gangqiang Yu: Conceptualization (lead); data curation (lead); formal analysis (lead); funding acquisition (equal); methodology (lead); project administration (lead); validation (lead); writing – original draft (lead); writing – review and editing (supporting). **Nicolás F. Gajardo-Parra:** Data curation (equal); investigation (equal); methodology (equal); software (supporting); writing – original draft (supporting). **Min Chen:** Data curation (equal); methodology (equal); software (supporting); validation (equal). **Biaohua Chen:** Data curation (equal); formal analysis (equal); funding acquisition (lead); investigation (equal); methodology (equal); project administration (equal). **Gabriele Sadowski:** Project administration (equal); resources (supporting); software (supporting);

supervision (equal). **Christoph Held:** Conceptualization (equal); data curation (supporting); investigation (equal); methodology (equal); project administration (lead); resources (supporting); software (supporting); supervision (lead); validation (supporting); writing – review and editing (lead).

ACKNOWLEDGMENTS

This work was financially supported by the National Natural Science Foundation of China under the grant (No. 22008003) and the China Scholarship Council (CSC) under the grant (No. 202206545009). The authors acknowledge funding from the Deutsche Forschungsgemeinschaft (DFG, German Research Foundation) under Germany's Excellence Strategy – EXC 2033 – project number 390677874. Translation into German required: "Gefördert durch die Deutsche Forschungsgemeinschaft (DFG) im Rahmen der Exzellenzstrategie des Bundes und der Länder – EXC 2033 – Projektnummer 390677874 – RESOLV." Nicolás Gajardo's work was supported by the German Academic Exchange Service (DAAD) under the Graduate School Scholarship Programme, 2020 (57516591). Open Access funding enabled and organized by Projekt DEAL.

CONFLICT OF INTEREST STATEMENT

The authors declare no competing financial interest.

DATA AVAILABILITY STATEMENT

The data that support the findings of this study are available from the corresponding author upon reasonable request.

ORCID

Gangqiang Yu https://orcid.org/0000-0002-3595-6972
Nicolás F. Gajardo-Parra https://orcid.org/0000-0002-2238-1807
Biaohua Chen https://orcid.org/0000-0002-9871-9560
Gabriele Sadowski https://orcid.org/0000-0002-5038-9152
Christoph Held https://orcid.org/0000-0003-1074-177X

REFERENCES

1. Huang HM, Wang ZW, Dai CH, Guo J, Zhang XS. Volatile organic compounds emission in the rubber products manufacturing processes. *Environ Res*. 2022;212:113485.
2. Tan Y, Han SW, Chen Y, et al. Characteristics and source apportionment of volatile organic compounds (VOCs) at a coastal site in Hong Kong. *Sci Total Environ*. 2021;777:146241.
3. Yang Y, Luo H, Liu R, Li G, Yu Y, An T. The exposure risk of typical VOCs to the human beings via inhalation based on the respiratory deposition rates by proton transfer reaction-time of flight-mass spectrometer. *Ecotox Environ Safe*. 2020;197:110615.
4. Faber J, Brodzik K, Golda-Kopek A, Lomankiewicz D. Air pollution in new vehicles as a result of VOC emissions from interior materials. *Pol J Environ Stud*. 2013;22(6):1701-1709.
5. Bayn A, Feng X, Muellen K, Haick H. Field effect transistors based on polycyclic aromatic hydrocarbons for the detection and classification of volatile organic compounds. *ACS Appl Mater Interfaces*. 2013;5(8):3431-3440.
6. Kito AM, Pirbazari M, Badriyha BN, Ravindran V, Tyner R, Synolakis CE. Emissions of volatile and semi-volatile organic compounds and particulate matter from hot asphalts. *Environ Technol*. 1997;18(2):121-138.
7. Casset A, de Blay F. Health effects of domestic volatile organic compounds. *Rev Mal Respir*. 2008;25(4):475-485.
8. Wang HL, Wang Q, Gao YQ, et al. Estimation of secondary organic aerosol formation during a photochemical smog episode in Shanghai, China. *J Geophys Res - Atmos*. 2020;125(7):e2019JD032033.
9. Luo H, Jia L, Wan Q, An T, Wang Y. Role of liquid water in the formation of O_3 and SOA particles from 1,2,3-trimethylbenzene. *Atmos Environ*. 2019;217:116955.
10. Gao G, Liao Y, Li W, et al. Active surface RuO_x species originating from size-driving self-dispersion process for toluene catalytic combustion. *Chem Eng J*. 2022;441:136127.
11. Long G, Chen M, Li Y, et al. One–pot synthesis of monolithic Mn–Ce–Zr ternary mixed oxides catalyst for the catalytic combustion of chlorobenzene. *Chem Eng J*. 2019;360:964-973.
12. Zhao X, Liu X, Liu J, Chen J, Fu S, Zhong F. The effect of ionization energy and hydrogen weight fraction on the non-thermal plasma volatile organic compounds removal efficiency. *J Phys D Appl Phys*. 2019;52(14):145201.
13. Bo Z, Yan J, Li X, Chi Y, Cen K. Nitrogen dioxide formation in the gliding arc discharge-assisted decomposition of volatile organic compounds. *J Hazard Mater*. 2009;166(2–3):1210-1216.
14. Zang L, Wan Y, Zhang H, et al. Characterization of non-volatile organic contaminants in coking wastewater using non-target screening: dominance of nitrogen, sulfur, and oxygen-containing compounds in biological effluents. *Sci Total Environ*. 2022;837:155768.
15. Berardi C, Fibbi D, Coppini E, et al. Removal efficiency and mass balance of polycyclic aromatic hydrocarbons, phthalates, ethoxylated alkylphenols and alkylphenols in a mixed textile-domestic wastewater treatment plant. *Sci Total Environ*. 2019;674:36-48.
16. Jurkiewicz M, Musik M, Pelech R. Competitive adsorption of a binary VOC mixture from the gas phase onto activated carbon modified with malic acid. *Ind Eng Chem Res*. 2022;61(32):11947-11952.
17. Li X, Wang J, Guo Y, Zhu T, Xu W. Adsorption and desorption characteristics of hydrophobic hierarchical zeolites for the removal of volatile organic compounds. *Chem Eng J*. 2021;411:128558.
18. Feng D, Guo D, Zhang Y, et al. Functionalized construction of biochar with hierarchical pore structures and surface O-/N-containing groups for phenol adsorption. *Chem Eng J*. 2021;410:127707.
19. Yan X, Anguille S, Bendahan M, Moulin P. Ionic liquid membrane process for removal of volatile organic compounds from lab to industrial scale. *Chem Eng Technol*. 2021;44(11):2159-2163.
20. Lhuissier M, Couvert A, Kane A, Amrane A, Audic J-L, Biard P-F. Volatile organic compounds absorption in a structured packing fed with waste oils: experimental and modeling assessments. *Chem Eng Sci*. 2021;238:116598.
21. Golubev G, Sokolov S, Rokhmanka T, et al. High efficiency membranes based on PTMSP and hyper-crosslinked polystyrene for toxic volatile compounds removal from wastewater. *Polymers*. 2022;14(14):2944.
22. Zhang C, Gao X, Qin J, Guo Q, Zhou H, Jin W. Microporous polyimide VOC-rejective membrane for the separation of nitrogen/VOC mixture. *J Hazard Mater*. 2021;402:123817.
23. Gao Y, Zhang L, Huang A, et al. Unveiling the spatial and sectoral characteristics of a high-resolution emission inventory of CO_2 and air pollutants in China. *Sci Total Environ*. 2022;847:157623.
24. Cai M, An C, Guy C. A scientometric analysis and review of biogenic volatile organic compound emissions: research hotspots, new frontiers, and environmental implications. *Renew Sustain Energy Rev*. 2021;149:111317.
25. Heymes F, Manno-Demoustier P, Charbit F, Fanlo JL, Moulin P. A new efficient absorption liquid to treat exhaust air loaded with toluene. *Chem Eng J*. 2006;115(3):225-231.

26. Zeng S, Zhang X, Bai L, et al. Ionic–liquid-based CO_2 capture systems: structure, interaction and process. *Chem Rev*. 2017;117(14):9625-9673.
27. Shah MS, Tsapatsis M, Siepmann JI. Hydrogen sulfide capture: from absorption in polar liquids to oxide, zeolite, and metal–organic framework adsorbents and membranes. *Chem Rev*. 2017;117(14):9755-9803.
28. Zhang X, Ding X, Song Z, Zhou T, Sundmacher K. Integrated ionic liquid and rate–based absorption process design for gas separation: global optimization using hybrid models. *AIChE J*. 2021;67(10): e17340.
29. Zheng S, Zeng S, Li Y, et al. State of the art of ionic liquid-modified adsorbents for CO_2 capture and separation. *AIChE J*. 2022;68(2): e17500.
30. Ma D, Zhu C, Fu T, Ma Y, Yuan X. Performance and pressure drop of CO_2 absorption into task-specific and halide-free ionic liquids in a microchannel. *AIChE J*. 2022;68(6):e17613.
31. Xiong W, Shi M, Zhang X, Tu Z, Hu X, Wu Y. The efficient conversion of H_2S into mercaptan alcohols mediated in protic ionic liquids under mild conditions. *Green Chem*. 2021;23(20):7969-7975.
32. Cao Y, Zhang X, Zeng S, Liu Y, Dong H, Deng C. Protic ionic liquid-based deep eutectic solvents with multiple hydrogen bonding sites for efficient absorption of NH_3. *AIChE J*. 2020;66(8): e16253.
33. Zhang W, Luo J, Sun T, Yu F, Li C. The absorption performance of ionic liquids–PEG200 complex absorbent for VOCs. *Energies*. 2021; 14(12):3592.
34. Indra S, Subramanian R, Daschakraborty S. Interaction of volatile organic compounds acetone and toluene with room temperature ionic liquid at the bulk and the liquid–vacuum interface. *J Mol Liq*. 2021;331:115608.
35. Yu G, Dai C, Gao H, Zhu R, Du X, Lei Z. Capturing condensable gases with ionic liquids. *Ind Eng Chem Res*. 2018;57(36):12202-12214.
36. Xu R, Dai C, Mu M, et al. Highly efficient capture of odorous sulfur-based VOCs by ionic liquids. *J Hazard Mater*. 2021;402:123507.
37. Yu G, Mu M, Li J, et al. Imidazolium-based ionic liquids introduced into pi–electron donors: highly efficient toluene capture. *ACS Sustain Chem Eng*. 2020;8(24):9058-9069.
38. Wu B, Dai C, Chen B, Yu G, Liu N, Xu R. Ionic liquid versus traditional volatile organic solvent in the natural gas dehydration process: a comparison from a life cycle perspective. *ACS Sustainable Chem Eng*. 2019;7(23):19194-19201.
39. Wu B, Yu G, Liu N, Xu R, Chen B, Dai C. Deciphering the sustainability of an ionic liquid-based btx harvesting process from energetic, environmental, and economic perspectives. *ACS Sustainable Chem Eng*. 2021;9(2):863-873.
40. Abbott AP, Capper G, Davies DL, Rasheed RK, Tambyrajah V. Novel solvent properties of choline chloride/urea mixtures. *Chem Commun*. 2003;1:70-71.
41. Smith EL, Abbott AP, Ryder KS. Deep eutectic solvents (DESs) and their applications. *Chem Rev*. 2014;114(21):11060-11082.
42. Hansen BB, Spittle S, Chen B, et al. Deep eutectic solvents: a review of fundamentals and applications. *Chem Rev*. 2021;121(3):1232-1285.
43. Shi M, Xiong W, Zhang X, et al. Highly efficient and selective H_2S capture by task-specific deep eutectic solvents through chemical dual-site absorption. *Sep Purif Technol*. 2022;283:120167.
44. Zainal-Abidin MH, Hayyan M, Ngoh GC, Wong WF, Looi CY. Emerging frontiers of deep eutectic solvents in drug discovery and drug delivery systems. *J Control Release*. 2019;316:168-195.
45. van Osch DJ, Parmentier D, Dietz CH, van den Bruinhorst A, Tuinier R, Kroon MC. Removal of alkali and transition metal ions from water with hydrophobic deep eutectic solvents. *Chem Commun*. 2016;52(80):11987-11990.
46. Tran MK, Rodrigues M-TF, Kato K, Babu G, Ajayan PM. Deep eutectic solvents for cathode recycling of Li-ion batteries. *Nature Energy*. 2019;4(4):339-345.
47. Chen CC, Huang YH, Fang JY. Hydrophobic deep eutectic solvents as green absorbents for hydrophilic VOC elimination. *J Hazard Mater*. 2022;424:127366.
48. Mu ML, Zhang XF, Yu GQ, et al. Effective absorption of dichloromethane using deep eutectic solvents. *J Hazard Mater*. 2022;439: 129666.
49. Song Y, Chen S, Luo F, Sun L. Absorption of toluene using deep eutectic solvents: quantum chemical calculations and experimental investigation. *Ind Eng Chem Res*. 2020;59(52):22605-22618.
50. Dai CN, Chen M, Mu WB, et al. Highly efficient toluene absorption with pi–electron donor-based deep eutectic solvents. *Sep Purif Technol*. 2022;298:121618.
51. Gross J, Sadowski G. Perturbed-chain SAFT: An equation of state based on a perturbation theory for chain molecules. *Ind Eng Chem Res*. 2001;40(4):1244-1260.
52. Gross J, Sadowski G. Application of the perturbed-chain SAFT equation of state to associating systems. *Ind Eng Chem Res*. 2002;41(22): 5510-5515.
53. Klamt A. Conductor-like screening model for real solvents: a new approach to the quantitative calculation of solvation phenomena. *J Phys Chem*. 1995;99(7):2224-2235.
54. Yaws C, Yang H. To estimate vapor pressure easily. *Hydrocarbon Process*. 1989;68(10):65-68.
55. Cea-Klapp E, Polishuk I, Canales RI, Quinteros-Lama H, Garrido JM. Estimation of thermodynamic properties and phase equilibria in systems of deep eutectic solvents by PC-SAFT EoS. *Ind Eng Chem Res*. 2020;59(51):22292-22300.
56. Zubeir LF, Held C, Sadowski G, Kroon MC. PC-SAFT modeling of CO_2 solubilities in deep eutectic solvents. *J Phys Chem B*. 2016;120(9): 2300-2310.
57. Dietz CHJT, van Osch DJGP, Kroon MC, et al. PC-SAFT modeling of CO_2 solubilities in hydrophobic deep eutectic solvents. *Fluid Phase Equilib*. 2017;448:94-98.
58. Wertheim MS. Fluids with highly directional attractive forces. II. Thermodynamic perturbation theory and integral equations. *J Stat Phys*. 1984;35(1–2):35-47.
59. Wertheim MS. Fluids with highly directional attractive forces. I. Statistical thermodynamics. *J Stat Phys*. 1984;35(1–2):19-34.
60. Huang SH, Radosz M. Equation of state for small, large, polydisperse, and associating molecules. *Ind Eng Chem Res*. 1990;29(11):2284-2294.
61. Wolbach JP, Sandler SI. Using molecular orbital calculations to describe the phase behavior of cross-associating mixtures. *Ind Eng Chem Res*. 1998;37(8):2917-2928.
62. Yu G, Wei Z, Chen K, Guo R, Lei Z. Predictive molecular thermodynamic models for ionic liquids. *AIChE J*. 2022;68(4):e17575.
63. Hadj-Kali MK, Hizaddin HF, Wazeer I, El Blidi L, Mulyono S, Hashim MA. Liquid–liquid separation of azeotropic mixtures of ethanol/alkanes using deep eutectic solvents: COSMO-RS prediction and experimental validation. *Fluid Phase Equilib*. 2017;448:105-115.
64. Abranches DO, Larriba M, Silva LP, et al. Using COSMO-RS to design choline chloride pharmaceutical eutectic solvents. *Fluid Phase Equilib*. 2019;497:71-78.
65. Frisch M, Trucks G, Schlegel H, et al. *09, Revision D. 01*. Gaussian Inc.; 2009.
66. Perdew JP. Density–functional approximation for the correlation energy of the inhomogeneous electron gas. *Phys Rev B*. 1986;33(12): 8822-8824.
67. Schäfer A, Huber C, Ahlrichs R. Fully optimized contracted Gaussian basis sets of triple zeta valence quality for atoms Li to Kr. *J Chem Phys*. 1994;100(8):5829-5835.
68. Van Der Spoel D, Lindahl E, Hess B, Groenhof G, Mark AE, Berendsen HJ. GROMACS: fast, flexible, and free. *J Comput Chem*. 2005;26(16):1701-1718.

69. Martínez L, Andrade R, Birgin EG, Martínez JM. PACKMOL: a package for building initial configurations for molecular dynamics simulations. *J Comput Chem*. 2009;30(13):2157-2164.
70. Case D, Ben-Shalom I, Brozell S, et al. *AMBER 2018*. University of California; 2018.
71. Lu T, Chen F. Multiwfn: a multifunctional wavefunction analyzer. *J Comput Chem*. 2012;33(5):580-592.
72. Stephens PJ, Devlin FJ, Chabalowski CF, Frisch MJ. Ab initio calculation of vibrational absorption and circular dichroism spectra using density functional force fields. *J Comput Chem*. 1994;98(45):11623-11627.
73. Grimme S, Ehrlich S, Goerigk L. Effect of the damping function in dispersion corrected density functional theory. *J Comput Chem*. 2011;32(7):1456-1465.
74. Bennett CH. Efficient estimation of free energy differences from Monte Carlo data. *J Comput Phys*. 1976;22(2):245-268.
75. Tao DJ, Qu F, Li ZM, Zhou Y. Promoted absorption of CO at high temperature by cuprous-based ternary deep eutectic solvents. *AIChE J*. 2021;67(2):e17106.
76. Huang Y, Ouyang D, Ji Y. The role of hydrogen-bond in solubilizing drugs by ionic liquids: a molecular dynamics and density functional theory study. *AIChE J*. 2022;68(6):e17672.
77. Holbrey JD, Reichert WM, Nieuwenhuyzen M, Sheppard O, Hardacre C, Rogers RD. Liquid clathrate formation in ionic liquid–aromatic mixtures. *Chem Commun*. 2003;4:476-477.
78. Grimme S. Do special noncovalent π–π stacking interactions really exist? *Angew Chem Int Ed*. 2008;47(18):3430-3434.
79. Yu G, Xu R, Wu B, et al. Molecular thermodynamic and dynamic insights into gas dehydration with imidazolium-based ionic liquids. *Chem Eng J*. 2021;416:129168.

SUPPORTING INFORMATION

Additional supporting information can be found online in the Supporting Information section at the end of this article.

How to cite this article: Yu G, Gajardo-Parra NF, Chen M, Chen B, Sadowski G, Held C. Aromatic volatile organic compounds absorption with phenyl-based deep eutectic solvents: A molecular thermodynamics and dynamics study. *AIChE J*. 2023;69(5):e18053. doi:10.1002/aic.18053